NAR Genomics and Bioinformatics, 2024, **6**, lqae162
https://doi.org/10.1093/nargab/lqae162
Advance access publication date: 11 December 2024
Standard Article

In silico and *in vivo* analyses of a novel variant in *MYO6* identified in a family with postlingual non-syndromic hearing loss from Argentina

Paula I. Buonfiglio [1], Carlos D. Bruque [2], Lucía Salatino [3], Vanesa Lotersztein [4], Mariela Pace [1], Sofia Grinberg [1], Ana B. Elgoyhen [1,3], Paola V. Plazas [3,*] and Viviana Dalamón [1,*]

[1]Laboratorio de Fisiología y Genética de la Audición, Instituto de Investigaciones en Ingeniería Genética y Biología Molecular "Dr. Héctor N. Torres" (INGEBI), Consejo Nacional de Investigaciones Científicas y Técnicas (CONICET), Ciudad Autónoma de Buenos Aires, C1428ADN, Argentina
[2]Unidad de Conocimiento Traslacional Hospitalaria Patagónica, Hospital de Alta Complejidad SAMIC, El Calafate, Provincia de Santa Cruz, 9405, Argentina
[3]Instituto de Farmacología, Facultad de Medicina, Universidad de Buenos Aires, Ciudad Autónoma de Buenos Aires, C1121ABG, Argentina
[4]Servicio de Genética, Hospital Militar Central "Dr. Cosme Argerich", Ciudad Autónoma de Buenos Aires, C1426, Argentina

[*]To whom correspondence should be addressed. Tel: +5411 4783 2871 (Ext 15); Fax: +5411 4786 8578; Email: vividalamon@gmail.com
Correspondence may also be addressed to Paola V. Plazas. Tel: +5411 5950 9500 (Ext 2161); Email: pvplazas@gmail.com

Abstract

Hereditary hearing loss stands as the most prevalent sensory disorder, with over 124 non-syndromic genes and approximately 400 syndromic forms of deafness identified in humans. The clinical presentation of these conditions spans a spectrum, ranging from mild to profound hearing loss. The aim of this study was to identify the genetic cause of hearing loss in a family and functionally validate a novel variant identified in the *MYO6* gene. After Whole Exome Sequencing analysis, the variant c.2775G>C p.Arg925Ser in *MYO6* was detected in a family with postlingual non-syndromic hearing loss. By protein modeling a change in the electrostatic charge of the single alpha helix domain surface was revealed. Through a knockdown phenotype rescue assay in zebrafish, the detrimental effects of the identified variant on the auditory system was determined. These findings underscore the significance of a comprehensive approach, integrating both *in silico* and *in vivo* strategies, to ascertain the pathogenicity of this candidate variant. Such an approach has demonstrated its effectiveness in achieving an accurate genetic diagnosis and in promoting a more profound comprehension of the mechanisms that underlie the pathophysiology of hearing.

Graphical abstract

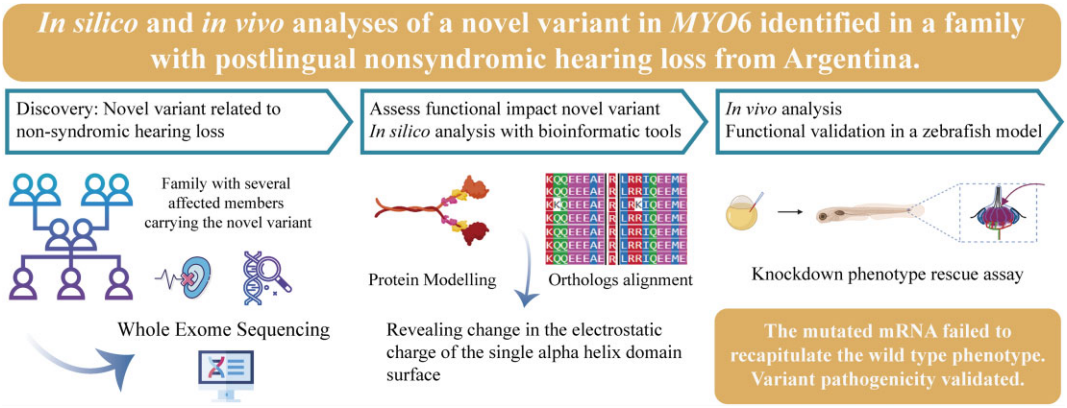

Introduction

Hearing loss (HL) is a highly prevalent and heterogeneous disorder that affects approximately 466 million people and 1–2 out of 1000 infants, with 50% of cases resulting from genetic factors (1,2). It has been estimated that 60–80% of congenital or prelingual forms of deafness are of genetic origin, and most

Received: September 17, 2024. **Revised:** October 23, 2024. **Editorial Decision:** November 5, 2024. **Accepted:** November 6, 2024

of these genetic forms are monogenic and of autosomal recessive (AR) inheritance (DFNB), generally causing severe to profound hearing loss (3,4). The remaining forms are mostly of autosomal dominant (AD) inheritance (DFNA), and are generally associated with initially less severe, but later progressive hearing impairment. A substantial proportion, ranging from 70% to 80%, of individuals diagnosed with congenital HL do not manifest clinical signs in other systems and are thus categorized as non-syndromic (NSHL). Among these cases, the majority (approximately 80%) follow an AR inheritance pattern, other 12–15% being attributed to AD inheritance, 1–5% X-linked and another 1–5% to mitochondrial inheritance (5). More than 200 genes (i.e. ∼1% of all the coding genes) are involved in the hearing process. Therefore, it is not surprising that hereditary HL (HHL) displays substantial genetic heterogeneity (6). The genes responsible for more than 140 isolated (non-syndromic) and about 400 syndromic forms of deafness have already been discovered, encompassing cases from birth to early adulthood (7–9). Up to date, a total of 124 causative genes linked to non-syndromic HL have been reported, comprising 78 with a AR inheritance pattern, 51 with a AD pattern and 5 X-linked genes (some of which can result in both recessive and dominant hearing impairment) (8). Clinical, genetic and allelic heterogeneity are frequent and represent a major concern and a challenge for diagnosis. For instance, hearing loss is variable regarding age of onset and severity, and other clinical signs also show variable expressivity.

The advent of next-generation sequencing technologies (NGS) has brought about a profound transformation in the diagnostic rate for HHL. This progress has resulted in the detection of novel variants within reported deafness genes and the unveiling of previously unidentified disease-causing genes. Consequently, Whole Exome Sequencing (WES) has emerged as an efficient and cost-effective alternative for achieving molecular diagnosis in cases of hearing impairment. In this study, we analyzed a family with autosomal dominant postlingual progressive non-syndromic HL by WES, and report a novel genetic variant (NM_004999.4) c.2775G>C p.Arg925Ser in the *MYO6* gene.

First, we applied the American College of Medical Genetics and Genomics and the Association for Molecular Pathology (ACMG/AMP) criteria to the variant, classifying it as likely pathogenic. Subsequently, we conducted both *in vitro* and *in vivo* experiments to examine the impact of the p.Arg925Ser variant on protein functionality, highlighting its potential implications in disease pathology and therapeutic strategies. We performed orthologous alignment of MYO6 protein sequences to assess conservation in the region. Additionally, we generated a structural model of the protein's three-helix bundle and single alpha helix (SAH) regions to investigate alterations in electrostatic charge on the protein surface. We further evaluated protein functionality in zebrafish (*Danio rerio*) where the orthologous *myo6b* gene is expressed on the apical surface of lateral line hair cells, maintaining the proper structure of the stereocilia, and is required for the correct mechanotransduction process. We generated a morpholino-mediated *myo6b* knockdown phenotype and attempted to rescue it with co-injections of either synthetic human wild type-*MYO6* RNA or mutant *MYO6*-p.R925S RNA. Our results revealed a reduced functionality of the mutated protein, strongly suggesting the pathogenicity of the *MYO6* variant.

Our integrated approach, combining *in silico* structural analysis and *in vivo* experimentation, effectively demonstrates the influence and pathogenicity of the identified c.2775G>C p.Arg925Ser variant in MYO6 functionality. This work shows the importance of combining molecular strategies not only to provide an accurate molecular diagnosis to patients and families, but also to further understand the implications of novel variants in the function of the auditory system. This research contributes to the broader field of molecular biology and highlights the importance of considering genetic variation in understanding biological processes.

Materials and methods

Patients and clinical evaluation

We clinically and genetically investigated an Argentinean family comprising 13 members, with eight individuals presenting postlingual HL compatible with AD-NSHL over three generations (Figure 1). The index patient, Patient IV:1, had initially been diagnosed with moderate-severe HL at the age of five. Subsequent audiological examinations of other relatives and siblings showed that HL was progressive in all of them. Written informed consent was obtained from all participants or parents in the case of minors, and the study was approved by the institutional review board of the Ethics Committee of Fundación para la Lucha contra las Enfermedades Neurológicas de la Infancia (FLENI) [protocol number 04092020.V1-01122024]. This study was conducted in accordance with ethical standards set forth by the Institutional and/or National Research Committee adhering to the principles outlined in the 1964 Helsinki Declaration and its later amendments, or comparable ethical standards. Clinical evaluation was performed by a clinical geneticist and included: personal history, physical examination, audiometric information, age of hearing impairment onset, hearing thresholds, pedigree and genetic assessment. Environmental causes of HL (e.g. ototoxic drugs, infectious diseases, acoustic trauma) were ruled out for each affected member of the family. Audiological evaluation included auditory brainstem response (ABR), tympanometry, logo audiometry and pure-tone audiometry at four frequencies (0.5, 1, 2 and 4 kHz). The pure-tone average (PTA) was calculated from the audiometric thresholds. The severity of deafness was classified considering the following thresholds in decibels: mild (20–39 dB), moderate (40–69 dB), severe (70–89 dB) and profound (90 dB).

Five family members suffered verifiable different degrees of HL over the whole frequency range. Slightly sloping mild-moderate HL was present in four members (III-3, III-5, III-6 and IV-1), and severe-profound deafness developed in patient III-1 (Figure 2).

Whole exome sequencing and variant analysis

Genomic DNA was extracted from peripheral blood samples and collected in 5% ethylene-diamine tetraacetic acid (EDTA) using the cetyltrimethyl-ammonium bromide (CTAB) method (10). The quality and concentration of the extracted DNA were measured through both agarose gel electrophoresis and absorbance-based nucleic acid quantification (Thermo Scientific™-NanoDrop™). All samples were stored at –20°C.

WES was performed to sample from patient IV-1 as previously described (11), after precluding frequent variants in *GJB2* and *GJB6* by direct sequencing and PCR-Gap (12). Sequencing was performed using the SureSelect V5-Post kit (Agilent Technologies, Santa Clara, CA) and sequenced with 100-

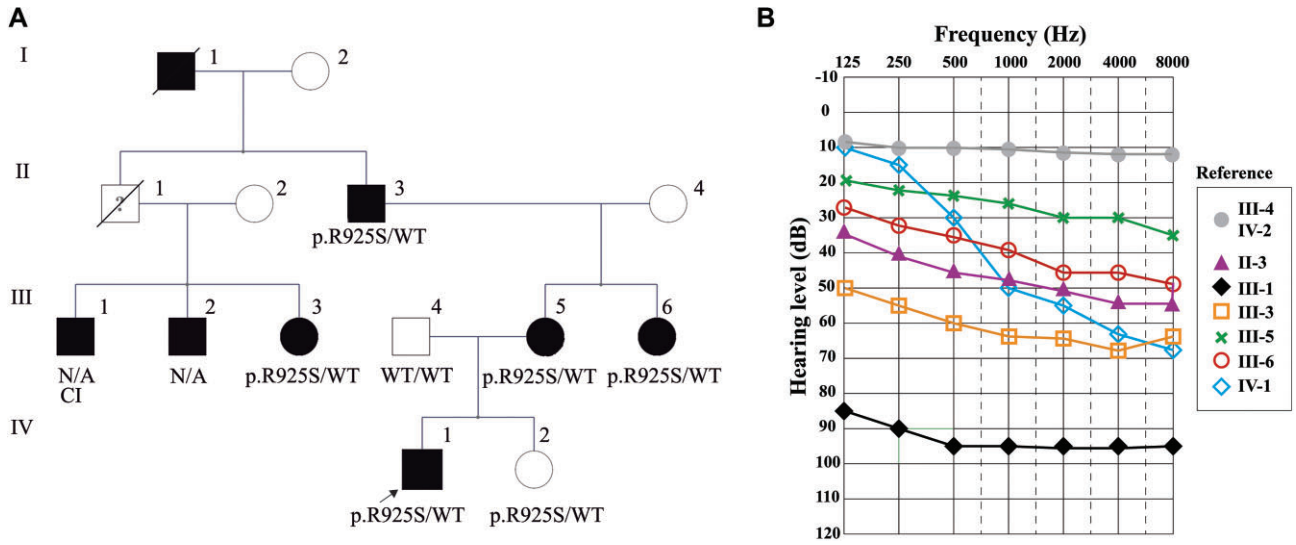

Figure 1. (**A**) Pedigree of the family harboring the causative variant p.Arg925Ser located within exon 26 of the *MYO*6 gene. Whole-exome sequencing was conducted on the proband IV-1, indicated by the arrow. All individuals with hearing impairment are in black. Seven members referred progressive postlingual hearing impairment (five available for the study), compatible with a dominant mode of inheritance. The genetic status 'WT' indicates wild type, 'NA': not available. (**B**) Audiograms of the affected family members who participated in the genetic test are shown, revealing the variable expressivity of the pathology. The patient's mother (III-5) and three aunts (III-1, III-3 and III-6) presented mild-moderate to severe and profound postlingual hearing impairment with onset in their thirties. They were all equipped with hearing aids, except III-1 that was cochlear implanted 'CI'.

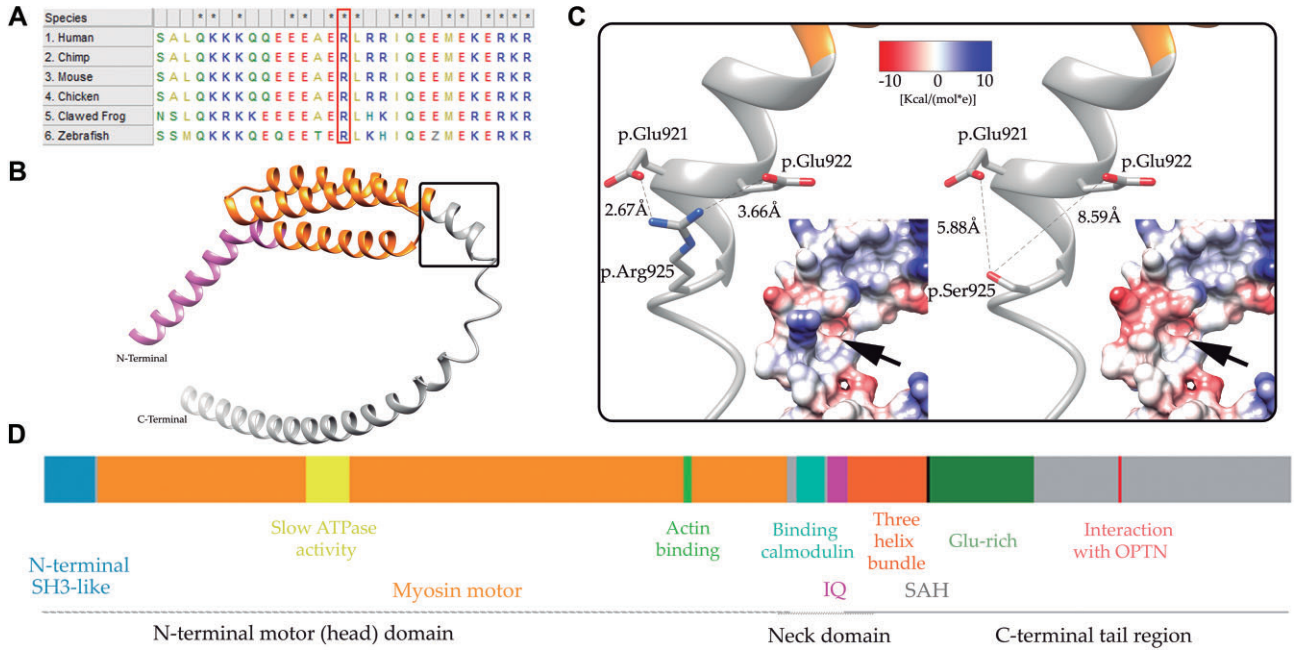

Figure 2. (**A**) Representative alignment across six MYO6 orthologous chordate sequences, revealing a 100% sequence identity for the Arg925 residue. (**B**) Structural modeling analysis of the IQ domain (pink), the three-helix bundle (orange) and the SAH (grey). (**C**) Evaluation of patterns on the protein surface showing the change in the electrostatic charge (arrow). Details of the interactions of the p.Arg925 or Ser925 within the SAH domain. The distances between p.Arg925 and p.Glu921/p.Glu922 are indicated as sticks in surface residues. (**D**) Schematic representation of MYO6 with the motor domain, neck domain and tail region. Residue numbers correspond to human MYO6, Uniprot entry Q9UM54.

base pair (bp) paired end reads on a HiSeq4000 (Illumina, San Diego, CA) to achieve a mean coverage of 80–100X, by the Macrogen Genome Sequencing Services (Macrogen, Korea). Thus, 97% of targeted reads had >10-fold coverage. Base calling, read mapping and annotation of variants were performed on the *GRCh37/hg19* genome from the University of California, Santa Cruz (UCSC) and data were processed according to the Genome-Analysis-Toolkit (GATK) best practices workflow. Variants that arose from the 222-known deafness genes (listed in Supplementary Table S1) were selected by filtering with an *in silico* panel using a homemade Python script pipeline. The missense, nonsense, insertion/deletion and splicing variants were selected from among the identified variants for further analysis. Variants were further selected as being less than 0.1% from the 1000 genome database and the gnomAD (Genome Aggregation Database:

http://gnomad.broadinstitute.org/). Direct Sanger sequencing was performed to confirm the selected variants.

The pathogenicity of the identified variants was evaluated according to the American College of Medical Genetics and Genomics and the Association for Molecular Pathology (ACMG/AMP) standards and guidelines, adapted following the latest hearing loss gene specific criteria of the ClinGen Hearing Loss Expert Panel (HL-EP) (13,14). Variants classified as 'pathogenic' and 'likely pathogenic' were considered as strong candidates for gene-associated hearing loss and further studied. The bioinformatic predictor REVEL algorithm (https://sites.google.com/site/revelgenomics) (15) with a score above 0.7 was considered to indicate a deleterious effect of missense variants. Information from population databases was gathered from ClinVar—https://www.ncbi.nlm.nih.gov/clinvar/, LOVD (Leiden Open Variation Database)—https://www.lovd.nl/ and Deafness Variation Database—https://deafnessvariationdatabase.org/.

To validate the candidate variants and assess their segregation within the family, Sanger sequencing was conducted for all five identified variants. A total of one hundred nanograms of genomic DNA was utilized to PCR-amplify the exonic regions of each gene, (data available upon request). Bidirectional DNA sequencing was executed using an automated sequencer (3730xl DNA Analyzer, Applied Biosystems, Foster City, CA, USA), Macrogen Genome Sequencing Services (Macrogen, Korea). The resulting sequences were subsequently analyzed through the CodonCodeAligner program (www.codoncode.com) and the BLAST (Basic Local Alignment Search Tool) NCBI interface (16). The final classification of the variants and their clinical significance was determined using the Variant Interpretation Platform for Genetic Hearing Loss (VIP-HL) (17). Final classification of variants, along with the pertinent clinical commentary of significance was submitted to ClinVar. The variant ultimately identified as causative of pathology in the family was located within the *MYO6* gene, using GeneBank accession number NG_009934.2. The genetic variant data that support the findings of this study are openly available in ClinVar at [http://www.clinvar.com/], reference number SUB14624738.

Sequence alignment and MYO6 protein structure

The *MYO6* gene is located on chromosome 6 (6q14.1) and consists of 35 exons that encode a 1294 amino acid protein referred to as myosin VI (Ensembl: ENSG00000196586; OMIM®: 600970; UniProtKB/Swiss-Prot: Q9UM54). Pathogenic genetic variants in *MYO6* are associated both with autosomal recessive and dominant hearing loss (DFNB37 and DFNA22, respectively). Myosins are actin-based motor molecules with ATPase activity. Myosin VI is a reverse-direction motor protein that moves toward the negative end of actin filaments and plays a crucial role in organizing the stereocilia bundle and maintaining anchorage of the cuticular plate of the stereocilia roots in hair cells (18,19). The structure of the MYO6 protein is divided into three regions: a N-terminal motor head domain (comprising the actin binding site, the myosin motor, the N-terminal SH3-like, and the ATP catalytic region), a neck domain (with a calmodulin-binding domain and a single IQ motif) and a C-terminal tail region (with a three-helix bundle region, an alpha helix SAH domain and a single globular domain required for interaction with other proteins, such as cargo binding) (GeneCards – the human gene database (www.genecards.org). Orthologous alignment of MYO6 was performed using the MEGA X software (20). Amino acid sequences for the myosin protein of six species were downloaded from the Uniprot database (https://www.uniprot.org/), accession ID numbers: Human Q9UM54, Chimpanzee H2R1E3, Mouse Q64331, Chicken Q9I8D1, Clawed Frog: A0A6I8RL33, Zebrafish F1R4R9. The mutated residue identified in the family is located in the SAH domain. Therefore, a structural model of the protein three-helix bundle and single alpha helix (SAH) regions (position: 835–984) of MYO6 was generated using AlphaFold2 ColabFold (21). To assess 3D structure prediction confidence quantitatively, AlphaFold2 provides per-residue pLDDT-predicted local distance difference test scores (scaled between 0 and 100). The selected structure had a pLDDT of 91.5 and a TM-score of 0.57 (22). The University of California, San Francisco (UCSF) Chimera program was used for structural visualization and the smoothed backbone-dependent rotamer library for structural interpretation (23,24). The ideogram of the MYO6 protein was generated with an in-house development program with the PyGame library in the Python 2.7 programming language (http://www.python.org) (25).

Animals

Zebrafish (*Danio rerio*) adults were maintained at 28°C on a 14 h light/10 h dark cycle and fed twice daily (26). Tg (Brn3c:mGFP) zebrafish line expressing GFP in hair cells were used (27). Embryos were obtained by natural crossing wild-type and Tg(Brn3c:GFP) adults and maintained according to standard protocols at 28.5°C in E3 medium (5 mM NaCl, 0.17 mN KCl, 0.25 mM $CaCl_2$, 0.33 mM $MgSO_4$). All experiments were conducted following the National Institutes of Health guide for the care and use of laboratory animal and approved by the Comité Institucional para el Cuidado y Uso de Animales de Laboratorio-CICUAL (Institutional Committee for the Care and Use of Laboratory Animals) of the School of Medicine, University of Buenos Aires, Argentina (resolution number 4081/04).

Gene knockdown and rescue in zebrafish

Previous studies have revealed two ohnologs for *myo6* in zebrafish, *myo6a and myo6b*, both homologues of the human *MYO6*. In particular, *myo6b* is expressed in the apical surface of zebrafish hair cells, maintaining the proper structure of the stereocilia, and is required for the correct mechanotransduction process (28,29).

To knock down the expression of the zebrafish *myo6b* gene, a calibration curve was constructed selecting a concentration of 3 ng of a previously described specific antisense morpholino oligonucleotide targeting the coding sequence, which offered the optimal balance between efficacy and mortality (Supplementary Figure S1). One-cell stage embryos were injected with Morpholino (MO): 5′-ACCCCACAATTACTCCACAGCTATT-3′ targeting the 5′-UTR of the coding sequence of *myo6b* and MO-CON: 5-ACgCCACtATTAgTCCtCAGgTATT-3′. All MOs were obtained from Gene Tools (Philomath, OR) (29).

For rescue studies, MOs were co-injected into one-cell zygotes of Tg(Brn3c:GFP) with 350 pg of either human WT-*MYO6* or mutant *MYO6*-p.R925S RNAs. Human WT

MYO6-cDNA was commercially obtained (GeneCopeia: EX-T0008-M03), while *MYO6*-p.R925S cDNA was obtained by site-directed mutagenesis using the Quick-Change Site-Directed Mutagenesis Kit (Stratagene). Human WT-*MYO6* and *MYO6*-p.R925S RNAs were synthesized *in vitro* using the RiboMax-Large Scale RNA Production System kit (Promega) followed by Poly(A) Tailing Kit (Thermofisher Scientific), according to the manufacturer's instructions. Optimization experiments were performed using different amounts of MOs and mRNAs (data not shown). The lowest doses able to induce a phenotype with minimal mortality rate were used: 3 ng of MO and 350 pg of mRNA. Following injection, embryos were reared in E3-medium at 28.5°C until 5 days post fertilization (dpf).

Phenotypic analysis

As previously reported, knock down of *myo6b* expression leads to the lack of an inflated swim bladder and a diminished labeling of lateral-line hair cells with 4-[4-(diethylamino)styryl]-N-methylpyridinium iodide (4-Di-2-Asp) dye, a cationic fluorophore that enters normal hair cells through intact mechanoelectrical transduction channels (29,30). Five dpf Tg (Brn3c:GFP) larvae were anesthetized with 0.04% MS-222 (Sigma Aldrich, St. Louis, MO), and mounted in 1% low-melting-point agarose. Images were captured under a light microscope (Nikon Y-TV 55) with a 4× objective. Staining with 4-Di-2-Asp was performed on live Tg (Brn3c:GFP) MO-injected larvae at 5 dpf. Zebrafish larvae were incubated for 4 minutes at room temperature in 200 μM 4-Di-2-Asp in E3 medium, washed four times with E3-medium, anesthetized with 0.04% MS-222 (Sigma Aldrich, St. Louis, MO) and then mounted on their lateral side in 1% low-melting-point agarose. Images of neuromasts situated between the otic vesicle and the eye were acquired with a 40× water-immersion objective lens on a laser-scanning confocal microscope (Leica TCS SPE) emitting light at 488 nm and 532 nm to visualize GFP and 4-Di-2-Asp, respectively. Stacks of confocal images at 0.78 μm intervals along the z-axis were taken and reconstructed with ImageJ software (31). Endogenous GFP expression in hair cells was used to delineate and visualize individual hair cells to later quantify 4-Di-2-Asp uptake. The optimal mold for accommodating the volume of the neuromasts was ascertained through the utilization of ImageJ's Auto-threshold tool (Li model). Fluorescence intensity was analyzed with the 3D ROI manager plugin (32). In each larval specimen, images of two neuromasts were taken. For each condition, $n \geq 8$ neuromasts from a minimum of four larvae were analyzed. Fluorescence intensity values were normalized to the averaged fluorescence intensity of images from wild-type un-injected larvae.

Statistical analysis

All analyses were performed using GraphPad Prism version 6.01 software (GraphPad Software, San Diego, California, USA, www.graphpad.com). Differences in morphological phenotypes were assessed through the chi-squared (χ^2) test. To evaluate the fluorescence intensity of neuromasts, a one-factor analysis of variance (ANOVA) was employed, followed by the Tukey Multiple Comparisons Test. Difference was considered statically significant at $P < 0.05$ for all analyses.

Results

Clinical description of the family

The proband is a seven-year-old boy, (denoted as IV-1 in Figure 1A), second child born to non-consanguineous parents with a documented family history of deafness, with no other signs nor symptoms affecting other organs. None of the family members had conductive hearing loss, tinnitus, episodes of dizziness, nor any vestibular signs. There was no clinical history of maternal infections during the pregnancy. The hearing impairment of the proband was considered to be moderate postlingual and stable when diagnosed at age five, showing a notable decline in high frequency auditory perception. His language development was adversely affected, but effectively managed through the use of hearing aids. The genetic analysis was conducted targeting the exons of 222 HL-related genes followed by analysis using the pipeline described in the material and methods section. The five years old younger sister (IV-2) exhibited normal hearing thresholds across the entire frequency range at the time of the study. Conversely, seven other family members displayed progressive postlingual hearing impairment (five available for the study), compatible with a dominant mode of inheritance (Figure 1A, B). Notably, the patient's mother (III-5), aunts (III-6 and III-3), and grandfather (II-3) exhibited mild-moderate to severe postlingual hearing impairment with onset in their thirties. They were equipped with hearing aids, while another aunt (III-1) received a cochlear implant.

Genetic analysis of the family

Four heterozygous candidate variants were selected in the proband of the family by WES in genes *SIX5*, *DMXL2*, *SEMA3E* and *MYO6*. Considering mode of inheritance, frequency threshold <1% in the gnomAD database, clinical data from ClinVar and evidence in mutation databases, all of them resulted as possible causes of the pathology. All variants were located in deafness genes of autosomal dominant inheritance, and those in *DMXL2*, *SEMA3E* and *MYO6* were novel. Variants in *SIX5*, *DMXL2* and *SEMA*3E genes were precluded when segregation resulted negative within the other members of the family by Sanger sequencing. Moreover, the genetic variant in *SIX5* had been previously reported in a patient with Branchiootorenal syndrome (BOR) (33) classified as VUS (variant of uncertain significance) based on the BS1, PS3_Supporting, and PP4 criteria, and the patients had no signs associated with this syndrome. The novel variant c.2775G>C p.Arg925Ser, located within the *MYO6* gene (NM_004999.4), demonstrated complete co-segregation in the four affected family members who were available for the molecular study.

Following the application of the ACMG/AMP guidelines and the specific criteria established by the Hearing Loss Expert Panel, the analysis of the *MYO6* c.2775G>C p.Arg925Ser variant resulted as follows: (i) 0.00031% (2/113 550) allele frequency based on non-European, non-Finnish alleles in the gnomAD database, with a 95% confidence interval, thereby fulfilling the PM2_Supp criteria; (ii) computational evidence alone did not provide evidence enough to apply the PP3 or BP4 criteria, as indicated by a REVEL score of 0.269; (iii) intrafamilial segregation of the variant revealed four positive members, meeting the criteria for PP1_Strong; (iv) based on the *in vivo* functional studies in zebrafish the variant fulfills

Table 1. Criteria applied for the *MYO6* NM_004999.4 c.2775G>C variant according to the ACMG/AMP guidelines and the specific criteria established by the Hearing Loss Expert Panel (HL-EP)

Allele frequency: 0.00031% (2/113 550)	Computational evidence: REVEL 0.269	Intrafamilial segregation: four positive members	Functional studies in zebrafish	Classification according to ACMG/HL-EP
PM2_Supp	–	PP1_Strong	PS3_Supporting	Likely Pathogenic

the PS3_Supporting criteria. Taking into account all criteria, the variant is classified as Likely Pathogenic (Table 1).

In silico analysis of the MYO6 p.Arg925Ser genetic variant

For a comprehensive assessment of the variant, we conducted a multiple-sequence alignment of MYO6 across orthologous genes from chordata species (human, chimp, mouse, chicken, frog and zebrafish) revealing 100% sequence identity for the Arg925 residue and the implicated region among the species analyzed (Figure 2A). This result is consistent with the findings obtained of 33 species through the analysis of the ortholog-based predictor PolyPhen (data not shown).

The structural modeling analysis of the three-helix bundle and the SAH regions (Figure 2B) indicates that the variant of interest is situated within the SAH domain. The Arg925Ser change generates a difference in relative distances between residue 925 and residues Glu922 and Glu921 within the domain (Figure 2C), causing potential instability in the region. A comparative evaluation of electrostatic charge patterns on the protein surface is shown in Figure 2D. In the wild-type model, Arg925 was positioned in the upper segment, surrounded by a region characterized by a low charge density. In contrast, the modeling of the protein harboring the mutated Ser925 residue revealed that the absence of the positively charged Arg925 resulted in a significant charge reorganization within the area, leading to a predominant negative charge configuration. The observed alteration in the electrostatic charge on the protein surface serves to bolster the theoretical underpinning of its pathogenicity. Given that the SAH domain plays a pivotal role in extending the arm of myosin VI and is crucial for its movement, specifically in the context of the step-walk mechanism, any modification in charge distribution could potentially disrupt the proper folding of the protein domain. As a consequence, this alteration is likely to have a deleterious impact on the functionality of MYO6.

In vivo analysis of the MYO6 genetic variant

To investigate the pathogenicity of the *MYO6* c.2775G>C p.Arg925Ser novel variant, we perform an *in vivo* study in zebrafish. The advantages of using this model system include its external fertilization, rapid development, optical transparency and genetic tractability. Like other fish and aquatic amphibians, zebrafish possess a series of neuromasts, mechanosensory receptors on the surface of the body that are very similar in structure and function to the sensory patches of the mammalian hair cells. These are arranged in precise lines along the fish body surface in the lateral line system (LL) and head and detect water movements and pressure changes relative to the animal's body (34). These hair cells are located superficially just beneath the fish skin facilitating high-resolution *in toto* live imaging (34,35).

We generated a morpholino-mediated *myo6b* knockdown phenotype and carried out its rescue with co-injections of synthetic human *MYO6* wild type RNA (MYO6-WT) and the mutant RNA (*MYO6*-p.Arg925Ser). To knock down the expression of the zebrafish *myo6b* gene, we used a previously described specific antisense morpholino oligonucleotide (MO) designed to target the 5′-UTR of the *myo6b* coding sequence (29). As a negative control, a morpholino (MO-CON) with five mismatched bases spanning the identical region was used. Consistent with Kappler *et al.*, nearly all (90%) larvae injected with MO exhibited a non-inflated swim bladder (Figure 3B). However, it is worth noting that in addition to the anticipated effects on swim bladder development, curved spine, pericardial edema, and yolk sac edema was observed in a small proportion of larvae injected with the MO.

Phenotypic screening was conducted on 5 dpf larvae, in both injected: MO-CON ($n = 81$ larvae); MO ($n = 110$ larvae); MO-WT-mRNA ($n = 92$ larvae); MO-R925S-mRNA ($n = 70$ larvae) and non-injected control groups: WT ($n = 105$ larvae). An overarching chi-squared (X^2) statistical analysis was executed comparing the following variables: inflated swim bladder (WT phenotype) versus non-inflated swim bladder. This study revealed a highly significant difference with a $P < 0.0001$ when comparing MO-CON with MO, MO-WT-mRNA and MO-R925S-mRNA. When comparing the non-injected and the MO-CON groups, no significant differences were observed ($P = 0.8776$). Additionally, no significant differences were detected when comparing morphant larvae with those co-injected with MO-WT-mRNA and MO-R925S-mRNA ($P = 0.8353$). Thus, most of the MO-WT-mRNA and MO-R925S-mRNA larvae exhibited a non-inflated swim bladder (91% and 88%, respectively) (Figure 3C).

Previous studies revealed that in zebrafish *myo6b* is expressed in hair cells and is required for the correct mechanotransduction process (20,21). In order to evaluate the potential impact of the c.2775G>C p.Arg925Ser variant on *MYO6* function we quantified the labeling of LL hair cells with 4-Di-2-Asp, a cationic fluorophore that enters hair cells via functional mechanotransduction channels (29,30). As expected and previously reported (29), larvae injected with MO displayed a decreased staining with 4-Di-2-Asp compared to larvae injected with MO-CON, due to the abnormal function of the mechanotransducer channels located on the apical surface of the hair cells (Figure 4A). Fluorescence intensity was measured on neuromasts situated between the otic vesicle and the eye (Figure 4A, red arrow) and normalized to the intensity per pixel. Confocal images showed the uptake of 4-Di-2-Asp dye (red) by LL hair cells of 5 dpf larvae (Figure 4C). The fluorescence intensity (fi) measured on neuromasts of larvae injected with MO (0.16 ± 0.09, $n = 10$ neuromasts from five larvae) was significantly lower than that of larvae injected with MO-CON (0.85 ± 0.24, $n = 8$ neuromasts from four larvae), $P < 0{,}0001$, ANOVA followed by Tukey multiple comparison-test (Figure 4C.1–2 and D).

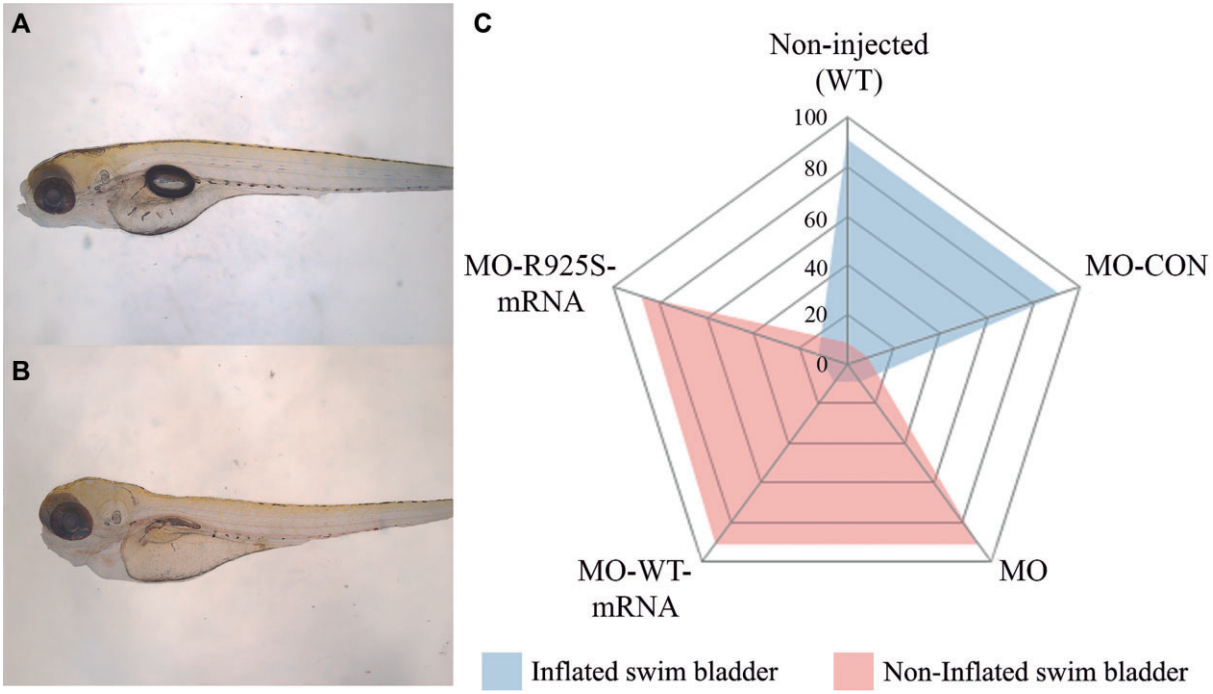

Figure 3. Morphological analysis of myo6b knockdown in zebrafish at 5 dpf: (**A**) lateral view of a larva with a wild-type phenotype, (**B**) lateral view of a *myo6b* morphant. Knockdown of myo6b caused non-inflation of the swim bladder. (**C**) Spider chart showing the percentages of the two variables analyzed: inflated and non-inflated swim bladder for each condition: WT, MO-CON, MO, MO-WT-mRNA, MO-R925S-mRNA.

Rescue experiments were performed by co-injecting MO with human wild-type *MYO6* mRNA (MO-WT-mRNA) or mutant *MYO6* mRNA (MO-p.R925S-mRNA) into embryos at the one-to-two-cell stage. We evidenced a partial rescue of the phenotype with the WT-mRNA, whereas p.R925S-mRNA failed to restore the knockdown phenotype, validating the pathogenic effect of the novel variant identified (Figure 4C.3–4 and D). Thus, 4-Di-2-Asp fluorescence intensity increased from 0.16 ± 0.09 to 0.43 ± 0.21 in MO and MO-WT-mRNA larvae, respectively ($n = 10$ neuromasts from five larvae for both conditions; $P < 0.0001$, ANOVA followed by Tukey multiple comparison-test). By contrast, co-injection of MO and human *MYO6* mRNA with the c.2775G>C p.Arg925Ser novel variant was unable to rescue the knockdown phenotype (MO: 0.16 ± 0.09 versus MO-p.R925S-mRNA: 0.21 ± 0.06, $n = 10$ neuromasts from five larvae for both condition, $P = 0.9032$, ANOVA test followed by Tukey multiple comparison-test).

Taken together, our results strongly support the hypothesis that the novel variant c.2775G>C p.Arg925Ser in *MYO6* gene affects the normal function of LL hair cells, thus providing consistent evidence of the pathogenic nature of this variant as a cause of postlingual progressive hearing loss.

Discussion

In the present study, we analyzed a family with several affected members with hearing impairment of autosomal dominant inheritance. All affected family members displayed progressive postlingual hearing loss of variable severity, characterized by a sloping audiometry pattern. Using WES, we identified the novel variant c.2775G>C, p.Arg925Ser within the *MYO6* gene. Myosin VI is a non-conventional myosin essential for the structural integrity and proper function of the hair cells of the inner ear (36,37). A recent study reported that the most prevalent mutated gene in European subjects with AD-NSHL is *MYO6* accounting for 20% of elucidated cases (38). Myosin 6 has two main functions: transport of cargo proteins and vesicles across actin filaments and the anchoring of the membrane of stereocilia to actin filaments (39,40). Hair cell function occurs primarily within two main structural domains, the apical hair bundle and the basal ribbon synapse. In response to sensory stimuli, apical hair bundles are deflected and this deflection opens mechanosensitive ion channels. This apical activity is essential to initiate hair cell depolarization, and opening of calcium channels at the synapse, leading to sensory evoked neurotransmission. Therefore, apical hair bundles must be intact and functional for proper hair cell synapse function (41).

The existence of absolute identity among 33 MYO6 SAH domain orthologous sequences implies strong selective pressure to maintain the sequence integrity of the domain. Thus, substitutions in the primary sequence of this domain could potentially disrupt its function and have deleterious effects on the organism, highlighting the functional significance and evolutionary importance of the SAH domain. The novel p.Arg925Ser substitution in the *MYO6* gene, is located in this region, between the IQ domain and the triple helix bundle, which together form the lever arm crucial for myosin VI's extension along the actin filament (42). Previous reports have highlighted the significance of the SAH domain in maintaining the stability of the adjacent triple helix domain, as well as bestowing upon myosin VI its ability to traverse the actin filament with its distinctive step size (43,44). In this context, it is pertinent to mention that previous studies involving *in vitro* assays and molecular dynamics simulations on myosin X have demonstrated the crucial role of SAH as a force spring during myosin movement (45). Furthermore, it has been reported

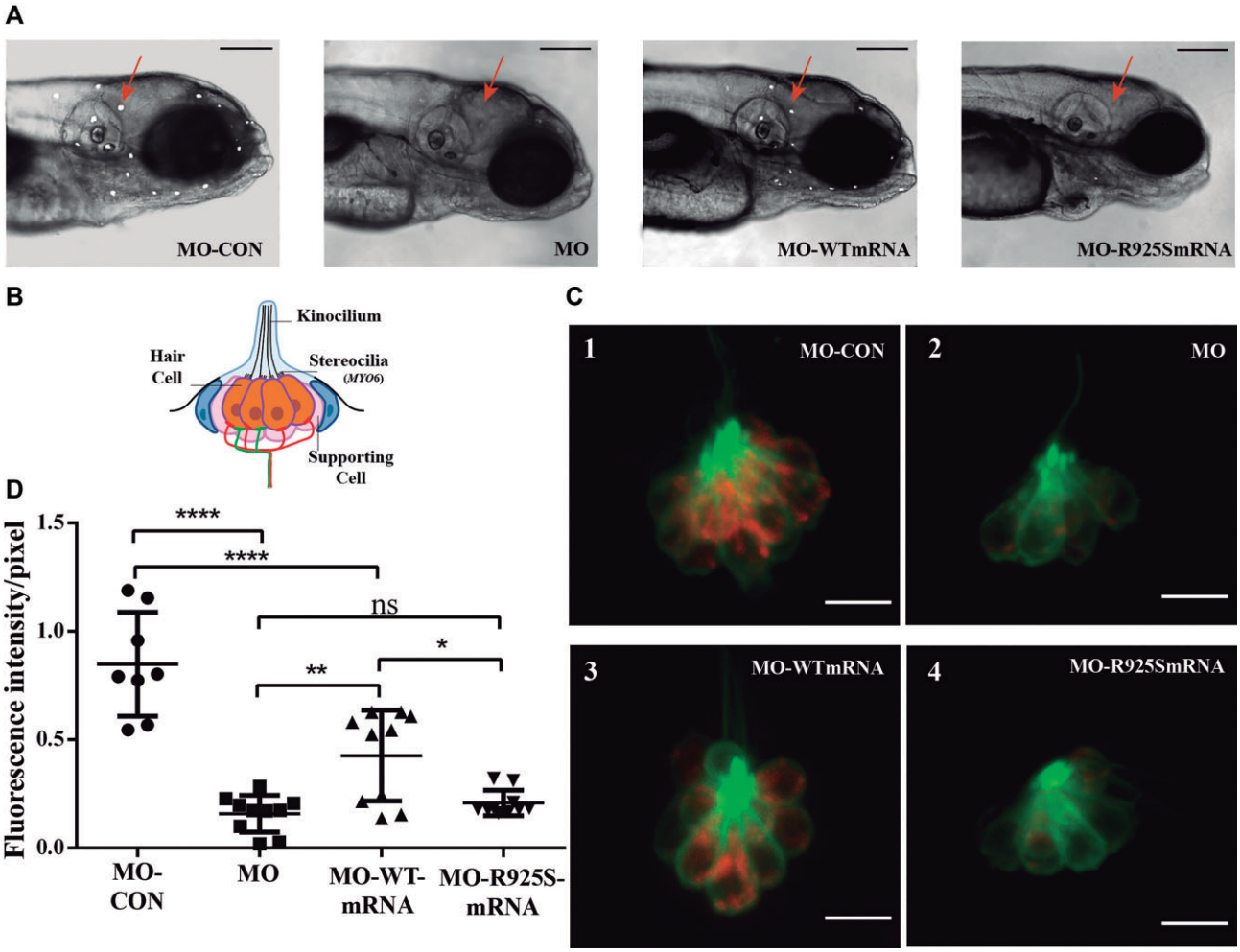

Figure 4. *In vivo* rescue assay of *myo6b* MO phenotype with human mRNAs. Coinjection of human wild-type *MYO*6 mRNA with *myo6b* MO resulted in partial rescue of the knockdown phenotype, whereas co injection of MO and human *MYO*6 mRNA with the c.2775G>C p.Arg925Ser novel variant (MO-p.R925S-mRNA) was unable to rescue the knockdown phenotype. (**A**) Lateral views of the head of 5dpf larvae labeled with 4-Di-2-Asp (10X magnification). Neuromasts stained are shown as white dots. Red arrows point at neuromasts situated between the otic vesicle and the eye, where fluorescence intensity measurements were performed. Scale bar: 200 μm. (**B**) Schematic depicts a lateral view of a neuromast. (**C**) Confocal images showing the uptake of 4-Di-2-Asp (red) by LL hair cells of 5 dpf Tg (Brn3c:GFP) larvae. GFP (green) is expressed in neuromast hair cells. Scale bar: 9 μm. (**D**) Box and whisker plot: fluorescence intensity per pixel (F/pix) normalized to the fluorescence intensity of non-injected larvae. ANOVA followed by Tukey multiple comparison-test,: $****P < 0.0001$, $***P < 0.001$, $**P < 0.01$, $*P < 0.05$, $n = 10$ neuromasts from five larvae, for each group.

that the region spanning from Lys915 to Arg940 residues may play a pivotal role in the dimerization of myosin VI (46). The SAH domain is characterized by an elevated concentration of charged residues, including arginine, lysine, and glutamic acid residues, which play a crucial function stabilizing the intra-helical interactions, thus facilitating the formation of salt bridges along the helix and conferring an exceptional stiffness to the helical domain (47,48). The novel *MYO6* variant identified in the present family leads to an amino acid substitution from a positively charged arginine to an uncharged serine at position 925. This observation is consistent with two other previous studies that reported pathogenic variants p.Leu926Gln and p.Arg928Cys located within the SAH domain, in which the mutated residues also changed their charge properties (49,50). Since this region is also predicted to be crucial for the proximal dimerization of the motor, the mutation is likely to impact stereocilia function that requires myosin VI to operate as a dimer (49). Our *in silico* structural analysis of the MYO6 SAH domain strongly suggests that the mutation Arg925Ser results in an alteration of the electrostatic charge on the protein surface, potentially causing a destabilization of the domain leading to structural changes that compromise its function. Consequently, it is plausible that the efficiency of the folding and unfolding of the SAH domain, which is instrumental in myosin VI's movement as a 'spring' (in its elastic and extensible function) and its dimerization, may be compromised. In this context, protein modeling emerges as a valuable tool for elucidating the mechanisms by which the p.Arg925Ser mutation impacts the proper function of the protein.

The *in vivo* zebrafish functional assay further confirmed the pathogenicity of the Arg925Ser mutation. Thus, the mutated mRNA was unable to rescue the knockdown phenotype, induced by a specific morpholino. In this regard, a significant proportion of the larvae injected with MO, failed to develop a swim bladder. Some reports have determined that the absence of an inflated swim bladder could be attributed to an elevated metabolic demand required for their survival, as well as the absence of access to an air-water interface, which is essential for bladder inflation and typically occurs within a specific developmental time frame (51,52). This is consistent with the

observation that under the present conditions morphant larvae exhibited impaired mobility, therefore limited to access to the air-water interface. Notably, a small proportion of morphant larvae displayed pericardial and yolk edema, a condition that has not been previously documented. This is in accordance with the observation that, although *myo6b* is mainly expressed in hair cell stereocilia, it has been also described in different zebrafish tissues such as heart, brain, eyes, intestine, which could account for the observed phenotype (28,29).

Our results showing that the WT-mRNA partially rescued the knockdown phenotype whereas the injection of the mutant p.Arg925Ser-mRNA failed to recapitulate the knockdown phenotype, confirm the pathogenicity of the MYO6 p.Arg925Ser genetic variant. A partial rescue of the knockdown phenotype with the WT mRNA is unsurprising given a previous report indicating that only 10% of larvae injected with WT zebrafish myo6-mRNA exhibited wild-type levels of fluorescence in labeled neuromasts with some neuromasts displaying a strong, while others a weak staining (29).

By means of *in silico* and *in vivo* functional analysis the c.2775G>C missense mutation p.Arg925Ser in *MYO6* was validated as the cause of HL in an Argentinean family with postlingual progressive hearing loss. This finding further expands the hearing loss mutation database and increases the comprehension of the molecular abnormalities caused by *MYO6* variants. Our functional validation confirms the pathogenic nature of the novel variant, further enhancing our comprehension of its role in the development of hearing loss within the studied family. These findings underscore the effectiveness of a comprehensive approach that combines molecular testing, *in silico* analysis, and *in vivo* experiments to investigate their implications within the auditory system.

Data availability

The genetic variant data that support the findings of this study are openly available in ClinVar at (http://www.clinvar.com/), reference number SUB14624738.

Supplementary data

Supplementary Data are available at NARGAB Online.

Acknowledgements

We thank the families for their kind contribution to this study. The authors want to thank Diego Weingier (INGEBI-CONICET) for his valuable insights and technical support with confocal microscopy.

Funding

National Agency for Scientific and Technological Promotion Grant [ANPCyT 'PICT-2018-00823' to A.B.E. and V.D.]; Multiannual Research Project grant of the National Council for Scientific and Technical Research- CONICET [PIP 2021-11220200102690CO to V.D. and P.P.]; P.B. is supported by a National Scientific and Technical Research Council Research Scholarship 'CONICET'. Institutional Review Board Statement: The study was conducted in accordance with the Declaration of Helsinki, and approved by the Ethics Committee of Fundación para la Lucha contra Enfermedades Neurológicas de la Infancia 'FLENI' [protocol number 04092020.V1], Buenos Aires, Argentina.

Conflict of interest statement

None declared.

References

1. Morton,C.C. and Nance,W.E. (2006) Newborn hearing screening — a silent revolution. *N. Engl. J. Med.*, **354**, 2151–2164.
2. Sordera y pérdida de la audición.
3. Shearer,A.E., Hildebrand,M.S., Schaefer,A.M. and Smith,R.J.H. (1999) Genetic hearing loss overview. In: Adam,M.P., Mirzaa,G.M., Pagon,R.A., Wallace,S.E., Bean,L.J.H., Gripp,K.W. and Amemiya,A. (eds.) *GeneReviews*. University of Washington, Seattle, Seattle (WA).
4. Koffler,T., Ushakov,K. and Avraham,K.B. (2015) Genetics of hearing loss: syndromic. *Otolaryngol. Clin. North Am.*, **48**, 1041–1061.
5. Morton,N.E. (1991) Genetic epidemiology of hearing impairment. *Ann. N. Y. Acad. Sci.*, **630**, 16–31.
6. Morgan,A., Lenarduzzi,S., Spedicati,B., Cattaruzzi,E., Murru,F.M., Pelliccione,G., Mazzà,D., Zollino,M., Graziano,C., Ambrosetti,U., *et al.* (2020) Lights and shadows in the genetics of syndromic and non-syndromic hearing loss in the Italian population. *Genes*, **11**, 1237.
7. Michalski,N. and Petit,C. (2022) Central auditory deficits associated with genetic forms of peripheral deafness. *Hum. Genet.*, **141**, 335–345.
8. Walls,W.D., Azaiez,H. and Smith,R.J.H. (2024) Hereditary hearing loss homepage. https://hereditaryhearingloss.org/ (17 September 2024, date last accessed).
9. Shearer,A.E., Hildebrand,M.S., Odell,A.M. and Smith,R. (2023) Genetic Hearing Loss Overview. https://www.ncbi.nlm.nih.gov/books/NBK1434/.
10. Murray,M.G. and Thompson,W.F. (1980) Rapid isolation of high molecular weight plant DNA. *Nucleic Acids Res.*, **8**, 4321–4325.
11. Buonfiglio,P.I., Bruque,C.D., Lotersztein,V., Luce,L., Giliberto,F., Menazzi,S., Francipane,L., Paoli,B., Goldschmidt,E., Elgoyhen,A.B., *et al.* (2022) Predicting pathogenicity for novel hearing loss mutations based on genetic and protein structure approaches. *Sci. Rep.*, **12**, 301.
12. Buonfiglio,P., Bruque,C.D., Luce,L., Giliberto,F., Lotersztein,V., Menazzi,S., Paoli,B., Elgoyhen,A.B. and Dalamón,V. (2020) GJB2 and GJB6 genetic variant curation in an Argentinean non-syndromic hearing-impaired cohort. *Genes (Basel)*, **11**, 1233.
13. Richards,S., Aziz,N., Bale,S., Bick,D., Das,S., Gastier-Foster,J., Grody,W.W., Hegde,M., Lyon,E., Spector,E., *et al.* (2015) Standards and guidelines for the interpretation of sequence variants: a joint consensus recommendation of the American College of Medical Genetics and Genomics and the Association for Molecular Pathology. *Genet. Med.*, **17**, 405–424.
14. Oza,A.M., DiStefano,M.T., Hemphill,S.E., Cushman,B.J., Grant,A.R., Siegert,R.K., Shen,J., Chapin,A., Boczek,N.J., Schimmenti,L.A., *et al.* (2018) Expert specification of the ACMG/AMP variant interpretation guidelines for genetic hearing loss. *Hum. Mutat.*, **39**, 1593–1613.
15. Ioannidis,N.M., Rothstein,J.H., Pejaver,V., Middha,S., McDonnell,S.K., Baheti,S., Musolf,A., Li,Q., Holzinger,E., Karyadi,D., *et al.* (2016) REVEL: an ensemble method for predicting the pathogenicity of rare missense variants. *Am. J. Hum. Genet.*, **99**, 877–885.
16. Altschul,S.F., Gish,W., Miller,W., Myers,E.W. and Lipman,D.J. (1990) Basic local alignment search tool. *J. Mol. Biol.*, **215**, 403–410.
17. Peng,J., Xiang,J., Jin,X., Meng,J., Song,N., Chen,L., Abou Tayoun,A. and Peng,Z. (2021) VIP-HL: semi-automated

ACMG/AMP variant interpretation platform for genetic hearing loss. *Hum. Mutat.*, **42**, 1567–1575.
18. Ahmed,Z.M., Morell,R.J., Riazuddin,S., Gropman,A., Shaukat,S., Ahmad,M.M., Mohiddin,S.A., Fananapazir,L., Caruso,R.C., Husnain,T., *et al.* (2003) Mutations of MYO6 are associated with recessive deafness, DFNB37. *Am. J. Hum. Genet.*, **72**, 1315–1322.
19. Melchionda,S., Ahituv,N., Bisceglia,L., Sobe,T., Glaser,F., Rabionet,R., Arbones,M.L., Notarangelo,A., Di Iorio,E., Carella,M., *et al.* (2001) MYO6, the human homologue of the gene responsible for deafness in Snell's waltzer mice, is mutated in autosomal dominant nonsyndromic hearing loss. *Am. J. Hum. Genet.*, **69**, 635–640.
20. Tamura,K., Peterson,D., Peterson,N., Stecher,G., Nei,M. and Kumar,S. (2011) MEGA5: molecular evolutionary genetics analysis using maximum likelihood, evolutionary distance, and maximum parsimony methods. *Mol. Biol. Evol.*, **28**, 2731–2739.
21. Mirdita,M., Schütze,K., Moriwaki,Y., Heo,L., Ovchinnikov,S. and Steinegger,M. (2022) ColabFold: making protein folding accessible to all. *Nat. Methods*, **19**, 679–682.
22. Jumper,J., Evans,R., Pritzel,A., Green,T., Figurnov,M., Ronneberger,O., Tunyasuvunakool,K., Bates,R., Žídek,A., Potapenko,A., *et al.* (2021) Highly accurate protein structure prediction with AlphaFold. *Nature*, **596**, 583–589.
23. Shapovalov,M.V. and Dunbrack,R.L., Jr (2011) A smoothed backbone-dependent rotamer library for proteins derived from adaptive kernel density estimates and regressions. *Structure*, **19**, 844–858.
24. Pettersen,E.F., Goddard,T.D., Huang,C.C., Couch,G.S., Greenblatt,D.M., Meng,E.C. and Ferrin,T.E. (2004) UCSF Chimera–a visualization system for exploratory research and analysis. *J. Comput. Chem.*, **25**, 1605–1612.
25. Kolomenski,J.E., Delea,M., Simonetti,L., Fabbro,M.C., Espeche,L.D., Taboas,M., Nadra,A.D., Bruque,C.D. and Dain,L. (2020) An update on genetic variants of the NKX2-5. *Hum. Mutat.*, **41**, 1187–1208.
26. Westerfield,M. (2000) The zebrafish book: a guide for the laboratory use of zebrafish Danio (Brachydanio) rerio.
27. Xiao,T., Roeser,T., Staub,W. and Baier,H. (2005) A GFP-based genetic screen reveals mutations that disrupt the architecture of the zebrafish retinotectal projection. *Development*, **132**, 2955–2967.
28. Seiler,C., Ben-David,O., Sidi,S., Hendrich,O., Rusch,A., Burnside,B., Avraham,K.B. and Nicolson,T. (2004) Myosin VI is required for structural integrity of the apical surface of sensory hair cells in zebrafish. *Dev. Biol.*, **272**, 328–338.
29. Kappler,J.A., Starr,C.J., Chan,D.K., Kollmar,R. and Hudspeth,A.J. (2004) A nonsense mutation in the gene encoding a zebrafish myosin VI isoform causes defects in hair-cell mechanotransduction. *Proc. Natl. Acad. Sci. U.S.A.*, **101**, 13056–13061.
30. Meyers,J.R., MacDonald,R.B., Duggan,A., Lenzi,D., Standaert,D.G., Corwin,J.T. and Corey,D.P. (2003) Lighting up the senses: FM1-43 loading of sensory cells through nonselective ion channels. *J. Neurosci.*, **23**, 4054–4065.
31. Schindelin,J., Arganda-Carreras,I., Frise,E., Kaynig,V., Longair,M., Pietzsch,T., Preibisch,S., Rueden,C., Saalfeld,S., Schmid,B., *et al.* (2012) Fiji: an open-source platform for biological-image analysis. *Nat. Methods*, **9**, 676–682.
32. Ollion,J., Cochennec,J., Loll,F., Escudé,C. and Boudier,T. (2013) TANGO: a generic tool for high-throughput 3D image analysis for studying nuclear organization. *Bioinformatics*, **29**, 1840–1841.
33. Hoskins,B.E., Cramer,C.H., Silvius,D., Zou,D., Raymond,R.M., Orten,D.J., Kimberling,W.J., Smith,R.J.H., Weil,D., Petit,C., *et al.* (2007) Transcription factor SIX5 is mutated in patients with branchio-oto-renal syndrome. *Am. J. Hum. Genet.*, **80**, 800–804.
34. Montgomery,J., Carton,G., Voigt,R., Baker,C. and Diebel,C. (2000) Sensory processing of water currents by fishes. *Philos. Trans. R. Soc. Lond. B Biol. Sci.*, **355**, 1325–1327.
35. Plazas,P.V. and Elgoyhen,A.B. (2021) The cholinergic lateral line efferent synapse: structural, functional and molecular similarities with those of the cochlea. *Front. Cell. Neurosci.*, **15**, 765083.
36. Avraham,K.B., Hasson,T., Sobe,T., Balsara,B., Testa,J.R., Skvorak,A.B., Morton,C.C., Copeland,N.G. and Jenkins,N.A. (1997) Characterization of unconventional MYO6, the human homologue of the gene responsible for deafness in Snell's waltzer mice. *Hum. Mol. Genet.*, **6**, 1225–1231.
37. Hertzano,R., Shalit,E., Rzadzinska,A.K., Dror,A.A., Song,L., Ron,U., Tan,J.T., Shitrit,A.S., Fuchs,H., Hasson,T., *et al.* (2008) A Myo6 mutation destroys coordination between the myosin heads, revealing new functions of myosin VI in the stereocilia of mammalian inner ear hair cells. *PLoS Genet.*, **4**, e1000207.
38. Del Castillo,I., Morín,M., Domínguez-Ruiz,M. and Moreno-Pelayo,M.A. (2022) Genetic etiology of non-syndromic hearing loss in Europe. *Hum. Genet.*, **141**, 683–696.
39. Sweeney,H.L. and Houdusse,A. (2007) What can myosin VI do in cells?*Curr. Opin. Cell Biol.*, **19**, 57–66.
40. Self,T., Sobe,T., Copeland,N.G., Jenkins,N.A., Avraham,K.B. and Steel,K.P. (1999) Role of myosin VI in the differentiation of cochlear hair cells. *Dev. Biol.*, **214**, 331–341.
41. Kindt,K.S. and Sheets,L. (2018) Transmission disrupted: modeling auditory synaptopathy in Zebrafish. *Front. Cell Dev. Biol.*, **6**, 114.
42. Mukherjea,M., Llinas,P., Kim,H., Travaglia,M., Safer,D., Ménétrey,J., Franzini-Armstrong,C., Selvin,P.R., Houdusse,A. and Sweeney,L., H. (2009) Myosin VI dimerization triggers an unfolding of a three-helix bundle in order to extend its reach. *Mol. Cell*, **35**, 305–315.
43. Spink,B.J., Sivaramakrishnan,S., Lipfert,J., Doniach,S. and Spudich,J.A. (2008) Long single alpha-helical tail domains bridge the gap between structure and function of myosin VI. *Nat. Struct. Mol. Biol.*, **15**, 591–597.
44. Knight,P.J., Thirumurugan,K., Xu,Y., Wang,F., Kalverda,A.P., Stafford,W.F., Sellers,J.R. and Peckham,M. (2005) The predicted coiled-coil domain of myosin 10 forms a novel elongated domain that lengthens the head. *J. Biol. Chem.*, **280**, 34702–34708.
45. Wolny,M., Batchelor,M., Knight,P.J., Paci,E., Dougan,L. and Peckham,M. (2014) Stable single α-helices are constant force springs in proteins. *J. Biol. Chem.*, **289**, 27825–27835.
46. Mukherjea,M., Ali,M.Y., Kikuti,C., Safer,D., Yang,Z., Sirkia,H., Ropars,V., Houdusse,A., Warshaw,D.M. and Sweeney,H.L. (2014) Myosin VI must dimerize and deploy its unusual lever arm in order to perform its cellular roles. *Cell Rep.*, **8**, 1522–1532.
47. Süveges,D., Gáspári,Z., Tóth,G. and Nyitray,L. (2009) Charged single α-helix: a versatile protein structural motif. *Proteins Struct. Funct. Bioinf.*, **74**, 905–916.
48. Batchelor,M., Wolny,M., Baker,E.G., Paci,E., Kalverda,A.P. and Peckham,M. (2019) Dynamic ion pair behavior stabilizes single α-helices in proteins. *J. Biol. Chem.*, **294**, 3219–3234.
49. Brownstein,Z., Abu-Rayyan,A., Karfunkel-Doron,D., Sirigu,S., Davidov,B., Shohat,M., Frydman,M., Houdusse,A., Kanaan,M. and Avraham,K.B. (2014) Novel myosin mutations for hereditary hearing loss revealed by targeted genomic capture and massively parallel sequencing. *Eur. J. Hum. Genet.*, **22**, 768–775.
50. Talebi,F., Mardasi,F.G., Asl,J.M. and Sayahi,M. (2017) Next-generation sequencing identifies three novel missense variants in ILDR1 and MYO6 genes in an Iranian family with hearing loss with review of the literature. *Int. J. Pediatr. Otorhinolaryngol.*, **103**, 103–108.
51. Woolley,L.D. and Qin,J.G. (2010) Swimbladder inflation and its implication to the culture of marine finfish larvae. *Rev. Aquacult.*, **2**, 181–190.
52. Goolish,E. (1999) Lack of gas bladder inflation by the larvae of zebrafish in the absence of an air–water interface. *J. Fish Biol.*, **55**, 1054–1063.

Received: September 17, 2024. **Revised:** October 23, 2024. **Editorial Decision:** November 5, 2024. **Accepted:** November 6, 2024